Mechanical Properties of Electrospun Silk Fibers

Mao Wang,[†] Hyoung-Joon Jin,[‡] David L. Kaplan,[§] and Gregory C. Rutledge*[,†]

Department of Chemical Engineering, Massachusetts Institute of Technology, Cambridge, Massachusetts 02139; Department of Polymer Science and Engineering, Inha University, Incheon 402-751, Korea; and Departments of Biomedical Engineering & Chemical and Biological Engineering, Tufts University, Medford, Massachusetts 02155

Received May 21, 2004; Revised Manuscript Received June 29, 2004

ABSTRACT: The morphology and microstructure of electrospun *B. mori* silk/poly(ethylene oxide) (PEO) fibers with diameters less than 1 μm were characterized using birefringence, wide-angle X-ray diffraction, differential scanning calorimetry, and atomic force microscopy (AFM). In the as-spun fibers, silk fibroin is present in a coil conformation due to rapid fiber formation during electrospinning. After treatment with methanol, the silk fibroin was transformed into a β-sheet-containing structure. Evidence for nanofibrils within the as-spun fibers was observed by AFM, and the PEO phase was dispersed as small, elongated islands within the silk fibroin matrix and oriented along the fiber direction. The mechanical properties of single fibers were characterized by AFM nanoindentation. The results were consistent with uniaxial tensile tests and with the morphological analysis. After methanol treatment and extraction with water, the electrospun silk fiber exhibits a lateral modulus of 8.0 GPa, within a factor of 2 of degummed native silk. The results provide additional insight into the nature of these reconstituted silk fibroin submicron diameter fibers, which have potential utility in a range of materials science and engineering applications.

Introduction

Tissue engineering has emerged as an interdisciplinary field that applies the principles of the engineering and life sciences to develop biological substitutes for restoring, maintaining, or improving the function of human tissue.[1] One of the main challenges in the field of tissue engineering/biomaterials is to design and engineer scaffolds or polymeric matrices that mimic the structure and biological functions of the natural extracellular matrix (ECM). The ECM is composed of a basement membrane and an interstitial complex consisting of a cross-linked network of multifibril collagens with diameters ranging from 15 μm down to 5 nm, interspersed with glycosaminoglycans.[2,3] Human cells adhere to and organize around these fibers, including those with diameters smaller than that of the cells.[4] Therefore, processing biocompatible polymers into nanofibers and nanofiber networks can begin to mimic some aspects of native ECM structure from a physical and biological perspective.[5−7]

Electrospinning is an effective method to produce fibers with diameters ranging from several nanometers to several micrometers.[8−10] A wide variety of polymers have been electrospun. Our focus here is on electrospun silk proteins due to their distinctive material and biological properties, such as high strength in fiber form, biocompatibility, good oxygen and water vapor permeability in film form, and biodegradability.[11] Silk fibroin film has been shown to exhibit cell attachment and growth comparable to collagen film.[12,13] *B. mori* silk has previously been electrospun to produce fibers with diameters as small as 6.5 nm from hexafluoro-2-propanol (HFIP)[14,15] or formic acid solutions.[3,16] We have previously shown that *B. mori* silk can be electrospun as a blend with PEO from aqueous solutions and that these electrospun silk protein fibers show promise as scaffolds for human bone marrow stem cell attachment and proliferation.[17,18] In tissue engineering, a scaffold should be capable of providing mechanical support for cell growth and migration. The mechanical properties of electrospun fibers can be manipulated through the appropriate selection of materials, varying solution composition, altering processing parameters, or utilizing postspinning treatments. However, because of the small diameters of electrospun fibers, the mechanical properties are usually obtained only for mats or yarns rather than for individual fibers.[19,20] The mechanical properties measured in this way depend strongly on fiber orientation within the material, bonding between fibers, and slip of one fiber over another. Taken together, these effects can easily mask the material-specific properties of the nanofibers that compose the mat or yarn. Furthermore, the modulus and strength of the materials cannot be calculated accurately due to the difficultly in determining the cross-sectional area of the mat or yarn due to porosity. Therefore, knowledge of mechanical properties of single fibers is desirable as a starting point in optimization of electrospinning conditions for specific fiber mechanical properties as well as for the design of useful materials composed of these fibers.

Nanoindentation using atomic force microscopy (AFM) is a technique that has been used to determine the mechanical properties of materials on a submicron scale.[21] The use of this technique to measure the mechanical properties of nanofibers is relatively new.[22] During AFM nanoindentation, the AFM probe tip is first lowered into contact with the sample, then indented into the sample surface, and finally lifted off the sample surface. The speed of indentation can be varied. Tip deflection is measured as a function of the vertical motion of the scanner, resulting in a curve that can be analyzed to provide information about local mechanical response.

The objective in the present study was to assess the mechanical properties of electrospun silk fibers using

[†] Massachusetts Institute of Technology.
[‡] Inha University.
[§] Tufts University.
* Corresponding author. E-mail: rutledge@mit.edu.

10.1021/ma048988v CCC: $27.50 © 2004 American Chemical Society
Published on Web 08/12/2004

the AFM nanoindentation technique as well as changes in the mechanical properties associated with various postprocessing treatments. To conduct these studies, first the morphology and microstructure of electrospun *B. mori* silk/poly(ethylene oxide) (PEO) fibers were assessed, before and after methanol treatment, and then again after extraction with water. The mechanical properties of these fibers prepared at different stages in the processing were determined by AFM nanoindentation. Native *B. mori* silk fiber was also investigated for comparison.

Experimental Part

Materials. Cocoons of *B. mori* silkworm silk were kindly supplied by M. Tsukada, Institute of Sericulture, Tsukuba, Japan. PEO with an average molecular weight of 9×10^5 g/mol (Aldrich) was used in the blends as previously reported.[17,18]

Preparation of Regenerated *B. mori* Silk Fibroin Solutions. *B. mori* silk fibroin was prepared using a modification of our earlier procedure.[17,18] Cocoons were boiled for 30 min in an aqueous solution of 0.02 M Na_2CO_3 and then rinsed thoroughly with water to extract the gluelike sericin proteins. The extracted silk was then dissolved in 9.3 M LiBr solution at 60 °C, yielding a 20% (w/v) solution. This solution was dialyzed in water using a Slide-a-Lyzer dialysis cassette (Pierce, MWCO 3500). The final concentration of aqueous silk solution was 8.0 wt %, which was determined by weighing the remaining solid after drying. Silk/PEO blends (80/20 wt %) in water were prepared by adding 8 mL of 5.0 wt % PEO (900 000 g/mol) into 20 mL of 8 wt % silk aqueous solution generating 7.1 wt % silk/PEO solutions. To avoid the premature formation of β-sheet structure during blending of the two solutions, the solutions were stirred gently at low temperature, 7 °C. Native silk fibers were prepared by boiling cocoons of *B. mori* for 30 min in an aqueous solution of 0.02 M Na_2CO_3 and then rinsing thoroughly with water to extract the gluelike sericin proteins. The fibers were dried at ambient conditions for 24 h and then in a vacuum at room temperature for another 24 h.

Electrospinning. Electrospinning was performed using a steel capillary tube with a 1.5 mm inside diameter tip as the spinnerette, mounted on an adjustable, electrically insulated stand as described earlier.[17,18,23] The capillary tube was maintained at a high electric potential for electrospinning and mounted in the parallel plate geometry.[23] The capillary tube was connected to a syringe filled with 10 mL of a silk/PEO blend solution. The electric potential, solution flow rate, and the distance between the capillary tip and the collection screen were adjusted so that a stable jet was obtained. By varying the distance between the capillary tip and the collection screen, either dry or wet fibers were collected on the screen.

Treatment of Electrospun Mats. Electrospun nonwoven mats from silk/PEO blend solutions were immersed into a 90/10 (v/v) methanol/water solution for 10 min at room temperature and then washed with water for 48 h at 37 °C to remove PEO from the mats. This process was performed in a shaking incubator at 50 rpm. Three versions of electrospun fibers were studied for mechanical properties: (a) the as spun fibers, (b) the fibers after treatment with methanol, and (c) the fibers after treatment with methanol and extraction with water.

Characterization. Images of electrospun fibers were obtained with a field emission gun scanning electron microscope (FESEM S-4200, Hitachi). Infrared spectra were measured with an ATR−FTIR (Bruker Equinox 55) spectrophotometer. Each spectrum was acquired in transmission mode on a ZnSe ATR crystal cell by accumulation of 256 scans with a resolution of 4 cm^{-1} and a spectral range of 4000−600 cm^{-1}. Wide-angle X-ray diffraction (WAXD) patterns were obtained using an X-ray diffractometer (Cu Kα) (Bruker D8) at 40 kV and 20 mA with a general area detector diffraction system (GADDS). The distance between the detector and the sample for WAXD was 47.0 mm.

Differential Scanning Calorimetry (DSC). The thermal transitions that occurred in native silk and the three types of electrospun fibers were characterized using a Q1000 modulated differential scanning calorimeter (TA Instrument Inc., DE). All the sample weights were about 4−6 mg, and all measurements were carried out under a nitrogen atmosphere. The specimens were scanned in three continuous thermal cycles at the same rate, 10 °C/min. In the first cycle, the specimens were heated from −100 to 140 °C to remove water, which shows up as a large endotherm around 100 °C, for the second and third cycles. After cooling to −100 °C, the specimens were heated again to 300 °C to complete the second cycle. In the third cycle, the specimens were cooled to −100 °C and then heated again to 300 °C. The thermographs of the second and third cycles were used for analysis.

Atomic Force Microscopy (AFM). *B. mori* silk/PEO nonwoven mats were embedded in a medium grade epoxy resin (London Resin Company Ltd., England) and cured for at least 72 h at room temperature. Transverse and longitudinal sections of the fibers were prepared by sectioning the nonwoven mats embedded in resin using an ultramicrotome (RMC Scientific Corp., Tucson, AZ) with a diamond knife. No evidence of knife damage to the sample was observed. Native *B. mori* silk fiber was also studied using the same method for comparison. A Nanoscope IV, Dimension 3100 AFM (Digital Instruments, Santa Barbara, CA), was employed in tapping mode with a RTESP single-beam silicon probe (Digital Instruments) to investigate the fibers. According to the manufacturer, the resonant frequency and force constant of the probe are 280−361 kHz and 30−40 N/m, respectively.

AFM Nanoindentation. The nanoindentation experiments were performed using the same AFM as above. A 22° compensation of the probe during the indentation was used to prevent the cantilever from plowing the surface laterally, typically along the x direction. Samples were prepared by sticking the nonwoven mats on a flat metal disk with a thin layer of epoxy glue. It was important to avoid diffusion of the glue into the fibers, which would otherwise reinforce the fibers. To avoid this problem, the epoxy glue was adhered first and cured for 5 min, almost to completion, before the nonwoven mats were placed on the material. Avoidance of glue infiltration into the fibers was confirmed by SEM observation of the nonwoven mats. The AFM indentation procedure consisted of three stages. First, the sample was inspected by AFM using tapping mode to locate the fiber for indentation. Then the scan area was set to 0 nm. The AFM was switched to force mode and the indentation performed. Finally, the AFM was switched back to tapping mode to image the indented area. All indentations were performed in the radial direction of the fiber.

Results and Discussion

Electrospinning. The pure silk solution (8 wt %) was not suitable for producing electrospun fibers, tending to break up into an electrospray instead. The addition of PEO (MW 900 000) to the silk fibroin solutions (8%) at the ratio of 1:4 by weight resulted in a solution whose viscoelasticity and surface tension were suitable for fiber formation, as we have previously reported.[17,18] The distance between the tip and the collector and the flow rate of the fluid were set at 21.5 cm and 0.03 mL/min, respectively, during electrospinning. As the voltage was gradually increased to 12.5 kV ($E = 0.6$ kV/cm), the drop at the end of the capillary tip elongated from a hemispherical shape into a cone shape and a jet was ejected from the tip of the cone. The jet then underwent a whipping instability to reduce the diameter dramatically before depositing on the collecting plate as a nonwoven mat.

The morphology and diameters of the electrospun fibers, before and after methanol treatment and after water extraction, were examined using SEM (Figure 1). The silk fibroin/PEO solution produced fine uniform fibers with 800 nm $\pm$ 50 average diameter.

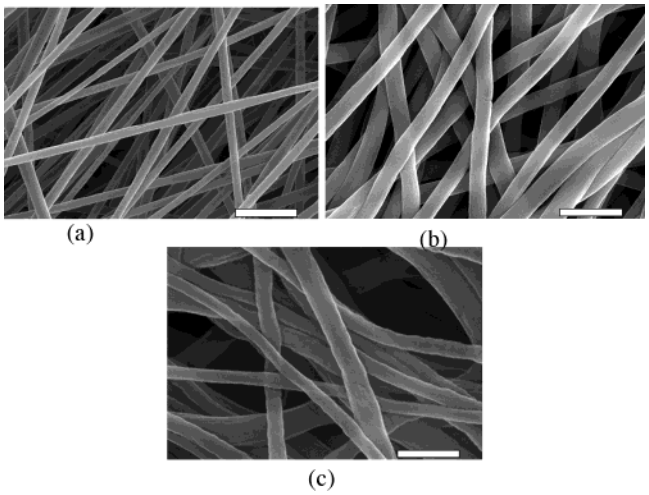

Figure 1. SEM images of *B. mori* silk/PEO fibers: (a) as-electrospun fiber (scale bar, 5 μm); (b) methanol-treated electrospun fiber (scale bar, 2.5 μm); (c) water-extracted electrospun fiber (scale bar, 2 μm).

Characterization of Electrospun Silk/PEO Fibers. The native silk spinning process by *B. mori* silkworm has been studied extensively.[24−26] Silk fibroin is synthesized in the posterior region of the gland and moves along in shearing flow to the anterior region of the gland with increasing concentration and speed. The fibroin solution in the anterior region forms a nematic liquid crystal phase prior to spinning, from which a silk filament is spun into air. The silk undergoes elongation after exiting the spinneret at a rate of 36−48 cm/min. The shearing and elongational flow during the spinning facilitates the orientation of the silk fibroin chains and the conversion of the soluble silk solution in the gland to the β-sheet found in the spun silk fiber.[27] In an analogous fashion, electrospinning of fibroin solutions results in a shear flow in the tube and capillary. After exiting the capillary, the jet experiences a whipping instability and is elongated up to 100 000 times in a short distance (up to 30 cm) in less than a second. The elongation rate can reach up to 10^4 s^{-1}.[8,28] The shear flow and high elongation rate during the electrospinning process are somewhat analogous to the native process in silkworm spinning. However, the rapid evaporation of the solvent and the short travel time of the jet in air (milliseconds) before deposition on the collecting device limits the time allowed for molecular rearrangement and crystallization. Thus, the degree of orientation and crystallization in electrospun nanofibers[29] could still be lower than in the case of native silk. In their work with silk fiber electrospun from HFIP, Zarkoob et al. reported that the fiber exhibited diffuse electron diffraction. After annealing, an oriented crystalline diffraction pattern was observed, but the silk fibers tend to degrade upon annealing at high temperature.[14,15] Figure 2 shows optical micrographs of both native silk and electrospun silk fibroin/PEO fibers under cross-polarized light. The detailed structure of native silk fibroin was reported by Marsh et al.[30] By rotating the fibers under cross-polarized optical microscopy, birefringence was observed for both fibers, indicating the presence of chain orientation and/or crystallization.[31,32]

Figure 3 shows WAXD diffraction patterns for the native silk fiber and the three different electrospun fibers. The WAXD patterns of as-spun fibers exhibit intense and sharp diffractions at 2θ = 19° and 23°,

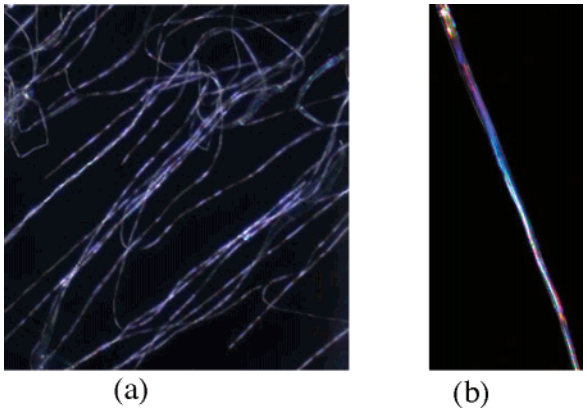

Figure 2. Birefringence of the fibers: (a) as-spun silk/PEO fiber (50× magnification, average diameter is 800 nm); (b) degummed native silk fiber (20× magnification, average diameter is 5 μm).

corresponding to 4.7 and 3.9 Å, respectively, which are characteristic of PEO crystals.[33] No group of diffraction peaks characteristic of the crystalline β-sheets of silk were observed, which indicates that the silk fibroin is amorphous in the as-spun fibers. This can be explained by the slow rate of crystallization for silk fibroin from water when compared to PEO. Fiber formation in electrospinning was completed in microseconds, allowing insufficient time for rearrangement of silk fibroin chains to form β-sheet crystals.[34] After methanol treatment, the PEO peaks disappeared, indicating that the PEO crystals were dissolved or disrupted by methanol at room temperature.[35] A broad Bragg reflection near $2\theta = 19.80°$ (crystalline spacing of 4.43 Å) was observed for the silk/PEO fibers after methanol treatment and water extraction. This peak is a characteristic feature of silk fibroin fiber with β-sheet structure and matches the native silk fiber (Figure 3d).[36] The rings observed in the WAXD data for the electrospun fibers are indicative of the random orientation of fibers in the nonwoven material, in contrast to the aligned sample of native silk fiber. FTIR data (Figure 4) confirm the conversion of silk from coil (1652.1, 1540.2, and 1521.0 cm^{-1}) to β-sheet structure (1698.0, 1627.7, 1621.2, 1523.5, 1513.2 cm^{-1}) after methanol treatment.[37,38]

The thermograms of the fibers from the second heating cycle are compared in Figure 5. A large endotherm at 250 °C was observed in all samples and is attributed to the destruction of the silk fibroin. For the native silk fiber, a transition was observed around 200 °C, which is attributed to a glass transition of the silk fibroin.[39,40] *B. mori* native silk is a semicrystalline material, and the percentage of crystallinity is about 65−70%.[41] For the silk/PEO as-spun fibers, a large endotherm was observed at ∼60 °C, which is attributed to the melting of the PEO crystals. Another transition was observed at 175 °C followed by a small exotherm. The transition is attributed to the glass transition of the silk fibroin and the small exotherm to cold crystallization of β-crystallites from the coil silk fibroin.[42,43] These results are consistent with the conclusions from WAXD that the PEO is partially crystallized and the silk uncrystallized in the as-spun silk/PEO fibers. For both the fibers treated with methanol and the fibers treated with methanol and subsequently extracted with water, no transitions were observed upon heating to the degradation point, as shown in Figure 5. The disappearance of the endotherm around 60 °C indicates that

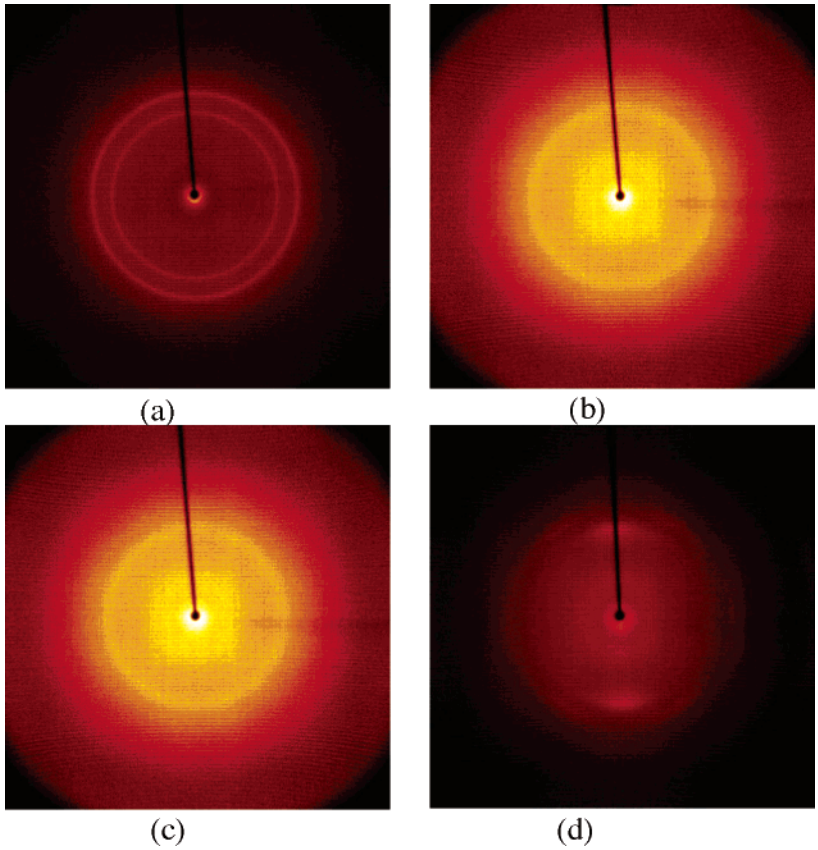

Figure 3. Wide-angle X-ray diffraction (WAXD) pattern of electrospun fiber mats from silk/PEO (80/20 wt %) solution: (a) as-spun fiber, (b) methanol-treated fiber, (c) PEO-extracted fiber, and (d) native silk fibers.

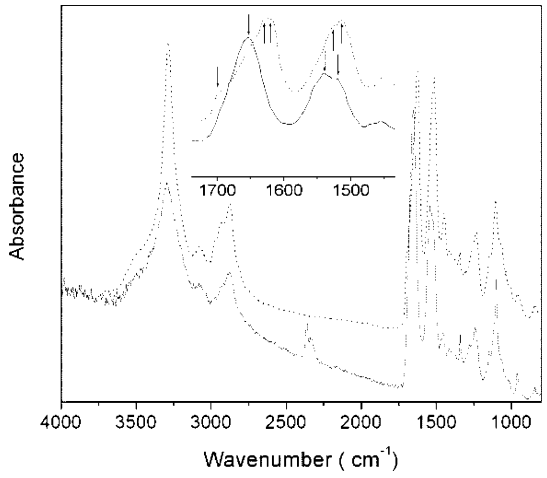

Figure 4. FTIR-ATR spectra of electrospun fiber from silk/PEO (80/20 wt %) solution: as-spun fiber (solid line); methanol-treated fiber (dotted line). The inset figure shows detail in the 1450−1750 cm^{-1} range, showing the transformation from peaks characteristic of the coil to those characteristic of the β-sheet (random coil: 1540.2 and 1521.0; silk I: 1652.1; silk II: 1697.1, 1627.7, 1621.2, 1523.5, and 1513.2 cm^{-1}).

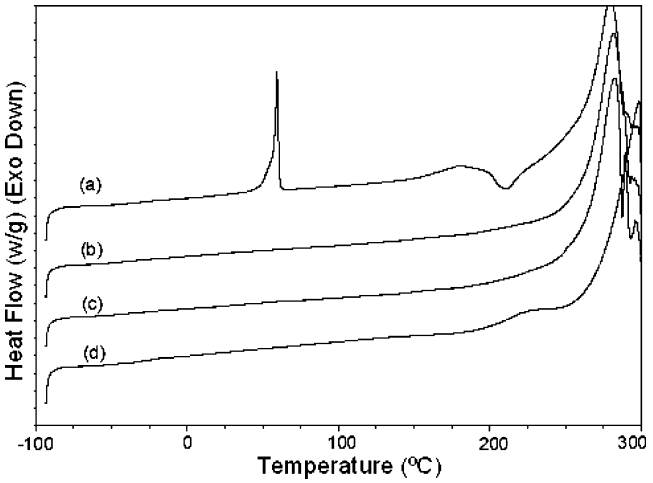

Figure 5. DSC thermographs of fibers from the second heating cycle: (a) as-electrospun fiber, (b) methanol-treated fiber, (c) water-extracted fiber, and (d) degummed native silk fiber.

the PEO crystals were dissolved or disrupted by the methanol treatment. The disappearance of the glass transition around 175 °C indicates that the noncrystalline silk component has been modified, most likely due to additional crystallization. These results are also consistent with the WAXD results. Figure 6 shows the thermograms of the fibers from the third heating cycle. An endothermic peak was observed at about 50 °C in all samples, which is attributed to the melting of the PEO crystals. The decreasing enthalpy of the peaks indicates the lower percentage of the PEO phase within the as-spun, methanol-treated, and water-extracted fibers, in that order. After water extraction, a small amount of PEO was still left within the fibers.

Microstructural Characterization. Figure 7 contains AFM images of *B. mori* silk fibroin/PEO as-spun fibers and the degummed native silk fiber. The diameters of the fibers and degummed native silk fiber are about 800 nm and 5 μm, respectively. The elliptical shape of the cross section of the silk/PEO fiber was due to the slanting of the embedded fiber within the epoxy resin relative to the cutting surface. Fine globular

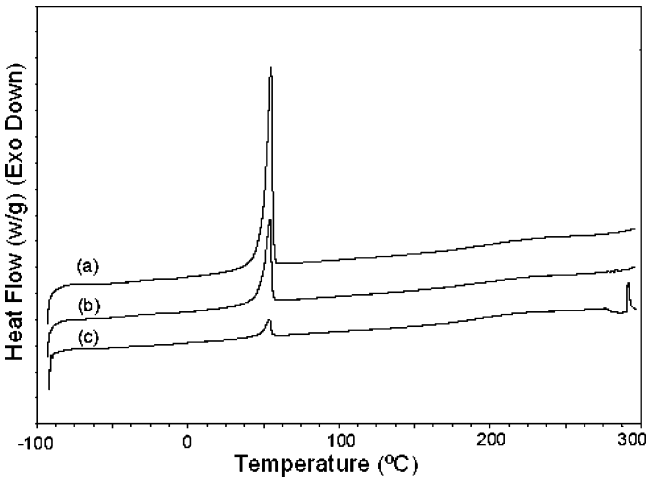

Figure 6. DSC thermographs of fibers from the third heating cycle: (a) as-electrospun fiber, (b) methanol-treated fiber, and (c) water-extracted fiber.

microstucture was observed in the cross section of both the as-spun silk/PEO fiber and the degummed silk fiber (Figure 7a,c). The diameter of the globular features is about 50 nm in the silk/PEO fiber and 120 nm in native silk fiber. Putthanarat et al. reported the width of silk fibrils in native silk fiber ranging from 90 to 170 nm.[44] In the longitudinal section of the fiber (Figure 7b) a feature diameter of 50 nm was observed. These morphological features probably relate to the recently reported mechanism of fibril formation during silk processing.[25] The fibroin molecules form micelles in solution due to chain folding and hydrophobic interactions. As the concentration of fibroin increases, the micelles coalescence and form globules. Elongation and alignment of globules and interactions among globules is promoted by shear during the spinning process, leading to fibrillar structures in the native silk fiber. The presence of nanofibrils in the electrospun fiber suggests that silk fibroin molecules in the silk/PEO solution during the electrospinning process undergo a similar mechanism, even though the solution is not in a liquid crystal phase prior to electrospinning.

Figure 8 contains SEM images of cross sections of electrospun fibers, which were fractured after immersion in liquid nitrogen for 1 h. No macroscopic phase separation was observed in the as-spun silk/PEO fibers (Figure 8a). The methanol-treated fibers are visualized in Figure 8b, which indicates the brittleness of the fibers after the treatment. In the water-extracted fibers, post methanol treatment, most of the PEO was removed, based on the DSC data as well as our prior X-ray photoelectron spectroscopy data.[17,18] After extraction of the PEO, a continuous phase fibroin fiber with a porous core structure was observed, indicating that the PEO phase was dispersed within this continuous fibroin matrix (Figure 8c,d). Figure 9a,b shows AFM images of the transverse and longitudinal sections of a silk/PEO

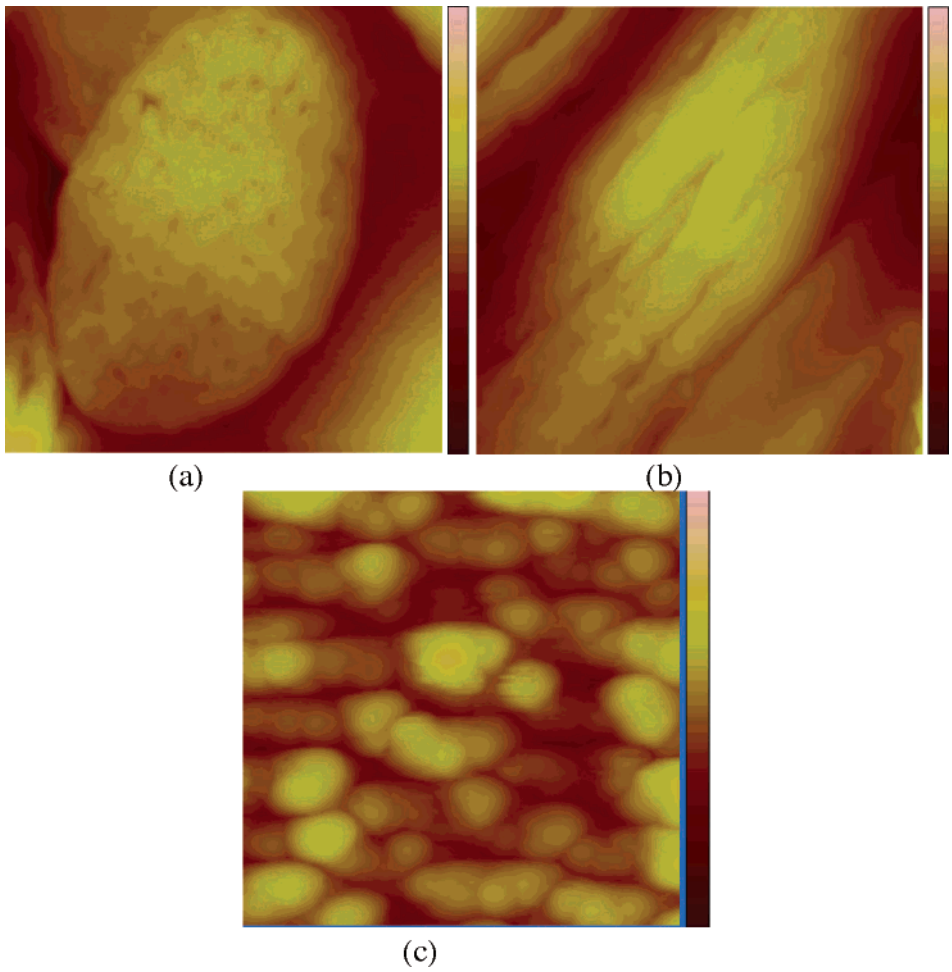

Figure 7. AFM investigation of the sections of fibers: (a) transverse section of silk/PEO fiber (size: 1 × 1 μm, color column: 0−200 nm); (b) longitudinal section of silk/PEO fiber (size: 1 × 1 μm, color column: 0−300 nm); (c) transverse section of degummed native silk fiber (size: 1 × 1 μm, color column: 0−200 nm).

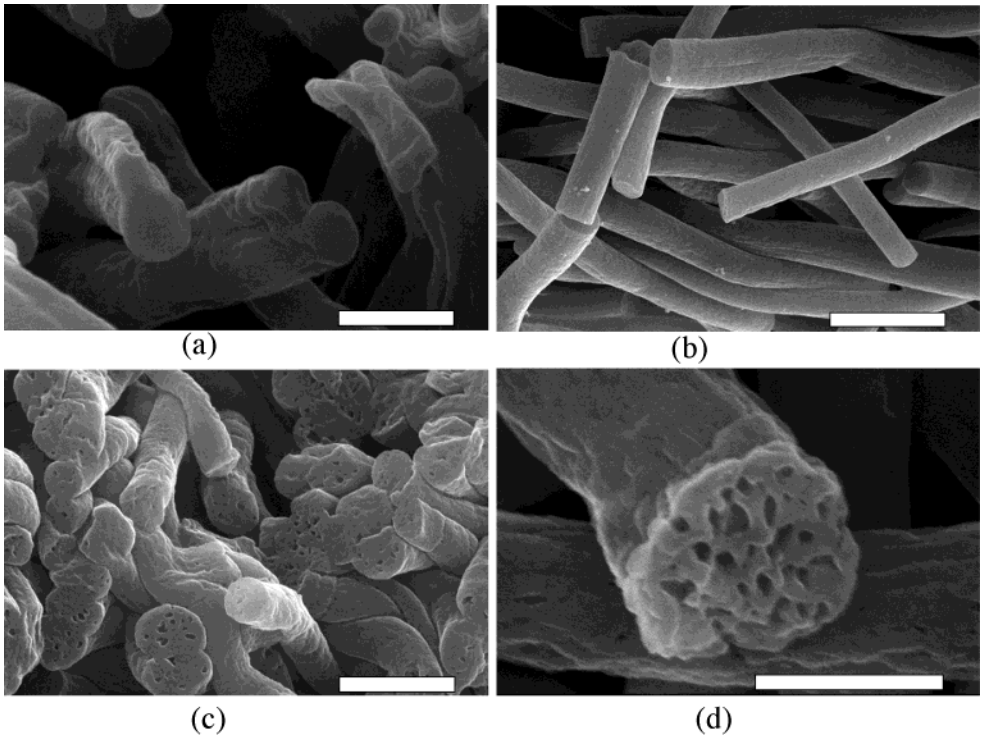

Figure 8. Cross-section images of electrospun fibers from silk/PEO (80/20 wt %) solutions: (a) as-spun fiber (scale bar, 1 μm); (b) methanol-treated fiber (scale bar, 2.5 μm); (c, d) PEO-extracted fiber (scale bar, 1 μm and 500 nm).

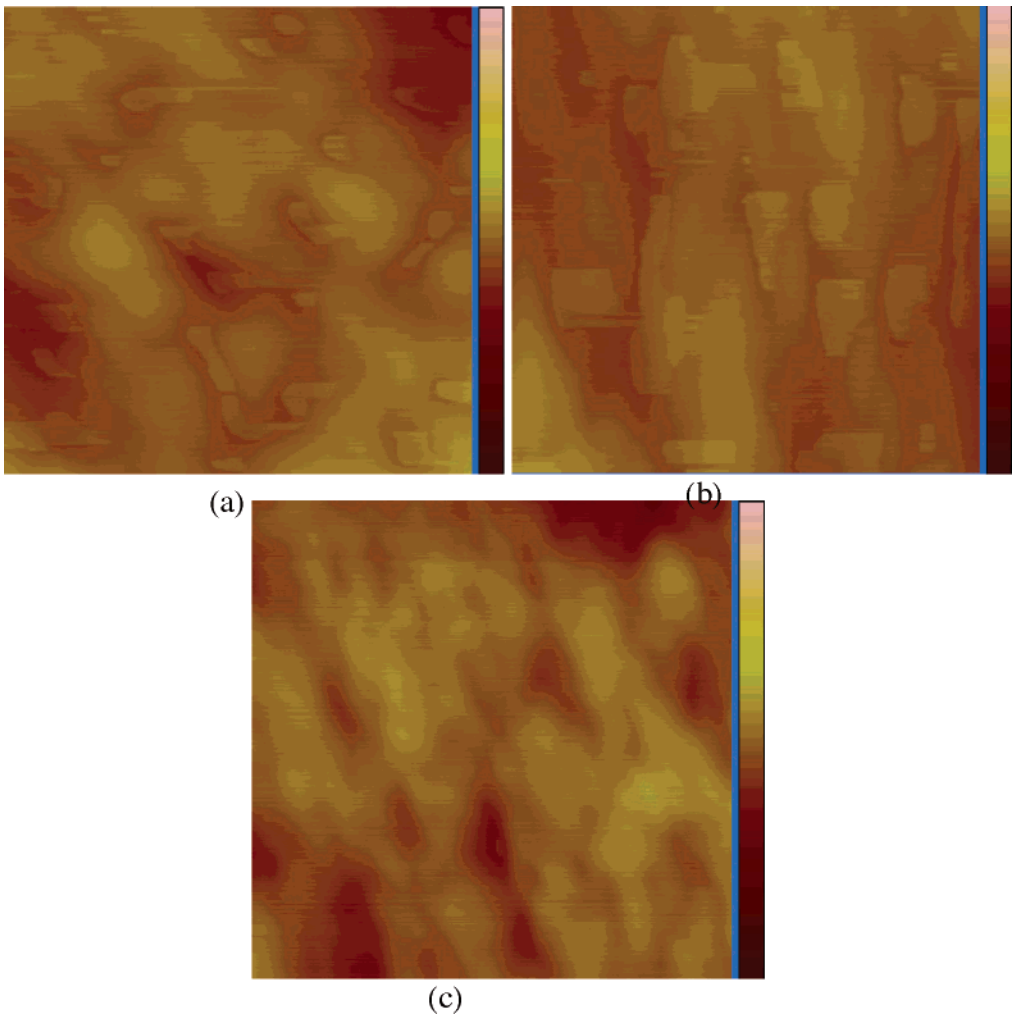

Figure 9. Close AFM images of the sections of silk/PEO fiber: (a) transverse section of fiber after methanol treatment (size: 200 × 200 nm, color column: 0−50 nm); (b) longitudinal section of fibers after methanol treatment (size: 200 × 200 nm, color column: 0−50 nm); (c) transverse section of fiber after water extraction (size: 200 × 200 nm, color column: 0−30 nm).

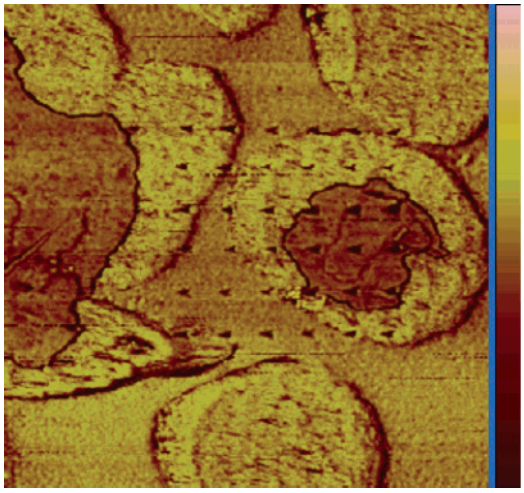

Figure 10. AFM phase image of the cross section of methanol-treated fiber (size: 2 × 2 μm, color column: 30°).

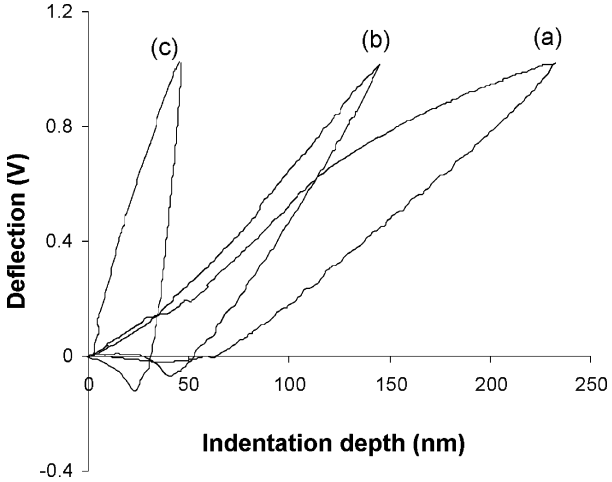

Figure 11. Representative loading and unloading curves of fibers: (a) as-spun fiber; (b) methanol-treated fiber; (c) water-extracted fiber.

fiber. The PEO phase is dispersed as small, elongated islands along the long axis (fiber direction) within the silk fibroin matrix. After extraction with water, most of the PEO phase has disappeared (Figure 9c).

It is interesting to note that the AFM phase image of the cross section of some of the methanol-treated silk fibroin/PEO fibers shows a skin-core structure (Figure 10). A series of AFM nanoindentation tests were performed across this cross section. The indentation results show that the fiber has a soft core and a hard shell. The hard shell is attributed to the crystallization of silk fibroin. This indicates that the methanol-induced crystallization proceeds gradually into the center of the fibers, as has been previously reported for reconstituted silkworm fibroin films used in enzyme-based sensors.[45−47]

AFM Nanoindentation. The elastic modulus of the fiber was evaluated using AFM nanoindentation according to the formula[48−51]

$$S = \frac{dP}{d\Delta Z_i}|_{P_{max}} = 2E^*\left(\frac{A}{\pi}\right)^{1/2} \quad (1)$$

where S is the slope of the unloading curve at P_{max}, P is the applied load, A is the contact area, ΔZ_i is the indentation depth, and E^* is the effective Young's modulus of the contact, as defined by

$$\frac{1}{E^*} = \frac{1-\nu_s^2}{E_s} + \frac{1-\nu_t^2}{E_t} \quad (2)$$

In eq 2, E_s and E_t are the elastic moduli, and ν_s and ν_t the Poisson ratios, of the sample and the tip, respectively. E_t and ν_t for the diamond tip are assumed to be 130 GPa and 0.2, respectively, corresponding to the bulk values for diamond.[51−53] AFM nanoindendation is applicable here due to the fact that the diameters of the fibers (>800 nm) are much larger than the diameter of the contact area (<10 nm).

The AFM indentation system is force controlled, as opposed to displacement controlled. P_{max} can be controlled to ±1% or better accuracy by setting an appropriate trigger set point of the deflection signal. In these experiments, the maximum trigger set point is 1 V for all the indentations. All indentations were made using the same loading/unloading rate, 1 Hz, to avoid the effects of rate-dependent deformation. Mica, with an elastic modulus of ~171 GPa and Poisson ratio of ~0.3,[51−53] was used as a standard to evaluate the penetration depth of the sample. For each sample, a minimum of 20 individual force curves was obtained.

Figure 11 shows representative curves of indentation depth into the sample vs deflection of cantilever for three different electrospun fibers. Table 1 shows the indentation data for the three different fibers. ΔZ_i is the displacement recovered from $P = P_{max}$ to $P = 0$. Z_t is the total indentation depth, including the inelastic and elastic deformation of the material. Z_t measures the penetration of the tip into the sample surface. Assuming the unloading recovery, ΔZ_i, is purely elastic,[54] the sequence of the elastic modulus of the three fibers, from highest to lowest, is $E_{\text{water extracted}} > E_{\text{methanol treated}} > E_{\text{as-spun}}$. This result is consistent with the results from the uniaxial tensile testing of nonwoven mats.[18] The mechanical properties of silk/PEO fibers are determined by the degree of orientation and crystallinity within the fibers. As with the WAXD and DSC analyses, the silk fibroin crystallinity of as-spun fibers is low due to the rapid fiber formation process during electrospinning. For this reason, the modulus is relatively low. Methanol treatment induces the transition of the silk fibroin from random coil into β-sheet crystals, and the modulus of the fiber increases. After extraction, most of the PEO phase was removed, which otherwise functioned as a plasticizer within the fiber, so the modulus of the fibers increases further.

The uncertainties on the cantilever stiffness and tip geometry of the AFM probe prevent calculating the absolute magnitude of moduli directly from eq 1.[55] To circumvent this problem, a reference flat sample of epoxy was indented using the same probe and parameters. The elastic modulus of the epoxy sample was determined independently using a Triboindenter with Berkovich-type indentation tip (Hysitron, Inc.). As shown in Figure 11, the slopes of the top portions of the unloading curves are constant, indicating the constant contact area at the initial portion of recovery. Thus, the unloading slope was computed by performing a linear fit of the top portion of the unloading curves.[56−58] However, it is noted that the unloading slope measurement depends on the portions of the curves used to create the linear fit. For this reason, it is very important to use the same number of data points in the linear

Table 1. AFM Nanoindentation Data of Fibers

	PEO/silk				
	as-spun	methanol-treated	water extracted	epoxy	degummed native silk fiber
Z_i (nm)	164.95 ± 12.59	112.30 ± 6.32	32.09 ± 11.95	42.02 ± 2.14	18.80 ± 1.18
Z_t (nm)	202.18 ± 22.39	135.65 ± 10.4	51.40 ± 13.53	132.55 ± 7.82	39.89 ± 4.70
modulus[a] (GPa)	0.75 ± 0.06	1.28 ± 0.08	8.00 ± 2.98	1.52 ± 0.12*	13.66 ± 0.85

[a] The modulus is determined independently by a triboindenter using a Berkovich tip.

approximation for all the indentations. In the present work, the 40% top portion of the unloading curves was used to determine the unloading slope. Assuming the tip geometry did not change during the indentations for all the samples, the relative changes in indent size could be used to relate contact area, which is characterized by a contact radius, r. Indent size was characterized by the lateral distance from the apex to the base of the triangular impression.[54,58] The indent sizes measured for the three different fibers are almost the same and are half the indent size for the epoxy sample. Poisson's ratio, ν, is assumed not to change significantly among the different type of fibers. Under these assumptions, the ratio of modulus of the different samples can be evaluated using the formula:

$$\frac{(\mathrm{d}P/\mathrm{d}\Delta Z_i)|_{P_{\max},1}}{(\mathrm{d}P/\mathrm{d}\Delta Z_i)|_{P_{\max},2}} = \frac{r_1 E_1}{r_2 E_2} \qquad (3)$$

The exact moduli of the fibers were obtained by comparison with the reference epoxy sample using eq 3 and are reported in Table 1. For comparison, a degummed native silk fiber was also indented using the same tip and methodology, and the modulus thus obtained was 13.66 ± 0.85 GPa. The native silk fiber was also indented using a Triboindenter with Berkovich-type indentation tip, and the modulus was found to be 14.38 ± 1.83 GPa. The data using different methods are in agreement, as judged by a statistical analysis of least significant difference, pairwise comparison, with a 0.05 level of significance. These results demonstrate that the AFM nanoindentation technique provides an effective tool to evaluate the mechanical properties of these types of fibers.

Conclusion

The morphology and microstructure of three different silk/PEO fibers (as-spun, methanol-treated, and water-extracted) were characterized by birefringence, WAXD, DSC, and AFM. In the as-spun fibers, PEO was crystallized while the silk fibroin was noncrystalline due to the rapid fiber formation process during electrospinning. After methanol treatment, silk fibroin was converted from coil into β-sheet crystals, while the PEO crystals dissolved or were disrupted in methanol. From AFM studies, nanofibrils formed within the as-spun fibers and the PEO phase was dispersed as small, elongated islands within the silk fibroin matrix. The mechanical properties of single electrospun fibers were investigated by AFM nanoindentation. The as-spun fibers exhibit the lowest modulus and the water extracted fibers exhibit the highest modulus. These results are consistent with the results of the tensile test and morphological analysis. The AFM nanoindentation technique provides an effective tool to evaluate the mechanical properties of individual electrospun fibers and provides a route forward to correlate solution variables and electrospinning and processing conditions on fiber features. These features can then be more directly related to cell and tissue outcomes when the mats and yarns are used in biomaterials related applications.

Acknowledgment. We thank the NSF (DMR), the NIH (EB003210), and Korea Research Foundation Grant (KRF-2003-003-D00103) for support of this research. This research was also supported by the U.S. Army through the Institute for Soldier Nanotechnologies, under Contract DAAD-19-02-D0002, with the U.S. Army Research Office.

References and Notes

(1) Langer, R.; Vacanti, J. P. *Science* **1993**, *260*, 920.
(2) Xu, C. Y.; Inai, R.; Kotaki, M.; Ramakrishna, S. *Biomaterials* **2004**, *259*, 877.
(3) Min, B. M.; Lee, G.; Kim, S. H.; Nam, Y. S.; Lee, T. S.; Park, W. H. *Biomaterials* **2004**, *25*, 1289.
(4) Laurencin, C. T.; Ambrosio, A. M. A.; Borden, M. D.; Cooper, J. A. *Annu. Rev. Biomed. Eng.* **1999**, *1*, 19.
(5) Li, W. J.; Laurencin, C. T.; Caterson, E. J.; Tuan, R. S.; Ko, F. K. *J. Biomed. Mater. Res.* **2002**, *60*, 613.
(6) Luu, Y. K.; Kim, K.; Hsial, B. S.; Chu, B.; Hadjiargyrou, M. *J. Controlled Release* **2003**, *89*, 341.
(7) Yoshimoto, H.; Shin, Y. M.; Terai, H.; Vacanti, J. P. *Biomaterials* **2003**, *24*, 2077.
(8) Doshi, J.; Reneker, D. H. *J. Electrostat.* **1995**, *35*, 151.
(9) Reneker, D. H.; Chun, I. *Nanotechnology* **1996**, *7*, 216.
(10) Fridrikh, S. V.; Yu, J. H.; Brenner, M. P.; Rutledge, G. C. *Phys. Rev. Lett.* **2003**, *90*, 144502.
(11) Santin, M.; Motta, A.; Freddi, G.; Cannas, M. *J. Biomed Mater. Res.* **1999**, *46*, 382.
(12) Minoura, N.; Aiba, S.-i.; Tsukuda, M.; Imai, Y. *J. Biomed. Mater. Res.* **1995**, *29*, 1215.
(13) Inouye, K.; Kurokawa, M.; Nishikawa, S.; Tsukuda, M. *J. Biochem. Biophys. Methods* **1998**, *37*, 159.
(14) Zarkoob, S.; Reneker, D. H.; Eby, R. K.; Hudson, S. D.; Ertley, D.; Adams, W. W. *Polym. Prepr.* **1998**, *39* (2), 244.
(15) Zarkoob, S.; Reneker, D. H.; Eby, R. K.; Hudson, S. D.; Ertley, D.; Adams, W. W. *Polymer* **2004**, *45*, 3973.
(16) Sukigara, S.; Gandh, M.; Ayutsede, J.; Micklus, M.; Ko, F. *Polymer* **2003**, *44*, 5721.
(17) Jin, H. J.; Fridrikh, S. V.; Rutledge, G. C.; Kaplan, D. L. *Biomacromolecules* **2002**, *3*, 1233.
(18) Jin, H. J.; Chen, J.; Karageorgiou, V.; Altman, G. H.; Kaplan, D. L. *Biomaterials* **2004**, *25*, 1039.
(19) Lee, K. H.; Kim, H. Y.; Ryu, Y. J.; Kim, K. W.; Choi, S. W. *J. Polym. Sci., Part B* **2003**, *41*, 1256.
(20) Pedicini, A.; Farris, R. J. *J. Vac. Sci. Technol.* **1989**, *A7*, 2906.
(21) Burnham, N. A.; Colton, R. J. *J. Vac. Sci. Technol.* **1989**, *A7* (4) Jul/Aug.
(22) Ko, F.; Gogotsi, Y.; Ali, A.; Naguib, N.; Ye, H. H.; Yang, G. L.; Li, C.; Willis, P. *Adv. Mater.* **2003**, *15*, 1161.
(23) Shin, Y. M.; Hohman, M. M.; Brenner, M. P.; Rutledge, G. C. *Polymer* **2001**, *42*, 9955.
(24) Vollrath, E.; Knight, D. P. *Nature (London) 410*, 541.
(25) Jin, H. J.; Kaplan, D. L. *Nature (London)* **2003**, *424*, 1057.
(26) Yamane, T.; Umemura, K.; Nakazawa, Y.; Asakura, T. *Macromolecules* **2003**, *36*, 6766.
(27) Trabbic, K. A.; Yager, P. *Macromolecules* **1998**, *31*, 462.
(28) Feng, J. J. *Phys. Fluids* **2002**, *14*, 3912.
(29) Dersch, R.; Liu, T.; Schaper, A. K.; Greiner, A.; Wendorff, J. H. *J. Polym. Sci., Part A* **2003**, *41*, 545.
(30) Marsh, R. E.; Covey, R. B.; Pauling, L. *Biochim Biophys. Acta* **1955**, *1*, 16.
(31) Fong, H.; Reneker, D. H. *J. Polym. Sci., Part B* **1999**, *37*, 3488.

(32) Chen, Z.; Forster, M. D.; Zhou, W.; Fong, H.; Reneker, D. H. *Macromolecules* **2001**, *34*, 6156.
(33) Tanaka, S.; Ogura, A.; Kaneko, T.; Murata, Y.; Akashi, M. *Macromolecules* **2004**, *37*, 1370.
(34) Sofia, S.; McCarthy, M. B.; Gronowicz, G.; Kaplan, D. L. *J. Biomed. Mater. Res.* **2001**, *54*, 139.
(35) Vandermiers, C.; Damman, P.; Dosiere, M. *Polymer* **1998**, *39*, 5627.
(36) Shen, Y.; Johnson, M. A.; Martin, D. C. *Macromolecules* **1998**, *31*, 8857.
(37) Valluzzi, R.; Szela, S.; Avtges, P.; Kirschne, D.; Kaplan, D. *J. Phys. Chem. B* **1999**, *103*, 11382.
(38) Wilson, D.; Valluzzi, R.; Kaplan, D. *Biophys. J.* **2000**, *78*, 2690.
(39) Magoshi, J.; Nakamura, S. *J. Appl. Polym. Sci.* **1975**, *19*, 1013.
(40) Nakamura, S.; Saegusa, Y.; Yamaguchi, Y.; Magoshi, J.; Kamiyama, S. *J. Appl. Polym. Sci.* **1986**, *31*, 955.
(41) Gohl, E. P. G.; Vilensky, L. D. *Textile Science*, 2nd ed.; Longman Cheshire: Melbourne, 1980.
(42) Magoshi, J.; Magoshi, Y.; Nakamura, S. *J. Polym. Sci., Polym. Phys. Ed.* **1981**, *19*, 185.
(43) Magoshi, J.; Magoshi, Y.; Nakamura, S.; Kasai, N.; Kakudo, M. *J. Polym. Sci., Polym. Phys. Ed.* **1977**, *15*, 1675.
(44) Putthanarat, S.; Stribeck, N.; Fossey, S. A.; Eby, R. K.; Adams, W. *Polymer* **2000**, *41*, 7735.
(45) Minoura, N.; Tsukada, M.; Nagura, M. *Polymer* **1990**, *31*, 265.
(46) Kuzuhara, A.; Asakura, T.; Tomoda, R.; Matsunaga, T. *J. Biotechnol.* **1987**, *5*, 199.
(47) Yoshimizu, H.; Asakura, T. *J. Appl. Polym. Sci.* **1990**, *40*, 127.
(48) Sneddon, J. N. *Int. J. Eng. Sci.* **1965**, *3*, 47.
(49) Pharr, G. M.; Oliver, W. C. *J. Mater. Res.* **1992**, *7*, 28.
(50) Pharr, G. M.; Oliver, W. C.; Brotzen, F. R. *J. Mater. Res.* **1992**, *7*, 613.
(51) Vanlandingham, M. R.; McKnight, S. H.; Palmese, G. R.; Eduljee, R. F.; Gillespie, J. W.; McCulough, R. L., Jr. *J. Mater. Sci., Lett.* **1997**, *16*, 117.
(52) Klapperich, C.; Komvopoulos, K.; Pruitt, L. *J. Tribol.* **2001**, *123*, 624.
(53) Kracke, B.; Damaschke, B. *Appl. Phys. Lett.* **2000**, *77*, 361.
(54) Vanlandingham, M. R.; Dagastine, R. R.; Eduljee, R. F.; McCullough, R. L.; Gillespie, J. W. *Composites: Part A* **1999**, *30*, 75.
(55) Vanlandingham, M. R.; McKnight, S. H.; Palmese, G. R.; Elings, J. R.; Huang, X.; Bogetti, T. A.; Eduljee, R. F.; Gillespie, J. W. *J. Adhes.* **1997**, *64*, 31.
(56) Doerner, M. F.; Nix, W. D. *J. Mater. Res.* **1986**, *1*, 601.
(57) Strojny, L. A.; Xia, X.; Tsou, A.; Gerberich, W. W. *J. Adhes. Sci. Technol.* **1998**, *12*, 1299.
(58) Drechsler, D.; Karbach, A.; Fuchs, H. *Appl. Phys. A: Mater. Sci. Process.* **1998**, *66*, S825.

MA048988V